Biochemistry

Communication

pubs.acs.org/biochemistry

Mechanistic Investigation of Oxidative Decarboxylation Catalyzed by Two Iron(II)- and 2-Oxoglutarate-Dependent Enzymes

Jhih-Liang Huang,[†] Yijie Tang,[‡] Cheng-Ping Yu,[†] Dev Sanyal,[†] Xinglin Jia, Xinyu Liu,*[,§] Yisong Guo,*[,‡] and Wei-chen Chang*[,†]

[†]Department of Chemistry, North Carolina State University, Raleigh, North Carolina 27695, United States

[‡]Department of Chemistry, Carnegie Mellon University, Pittsburgh, Pennsylvania 15213, United States

[§]Department of Chemistry, University of Pittsburgh, Pittsburgh, Pennsylvania 15260, United States

Supporting Information

ABSTRACT: Two non-heme iron enzymes, IsnB and AmbI3, catalyze a novel decarboxylation-assisted olefination to produce indole vinyl isonitrile, an important building block for many natural products. Compared to other reactions catalyzed by this enzyme family, decarboxylation-assisted olefination represents an attractive biosynthetic route and a mechanistically unexplored pathway in constructing a C=C bond. Using mechanistic probes, transient kinetics, reactive intermediate trapping, spectroscopic characterizations, and product analysis, we propose that both IsnB and AmbI3 initiate stereoselective olefination via a benzylic C−H bond activation by an Fe(IV)−oxo intermediate, and the reaction likely proceeds through a radical- or carbocation-induced decarboxylation to complete C=C bond installation.

Non-heme mononuclear iron(II)- and 2-oxoglutarate-dependent (Fe/2OG) enzymes catalyze a broad range of oxidative transformations involved in the regulation and biosynthesis of cellular metabolites.[1,2] Among these diverse transformations, the mechanism of hydroxylation has been most extensively investigated. This process is initiated by H atom abstraction (HAT) by an Fe(IV)−oxo species, followed by a rapid C−O bond formation between the substrate radical and Fe(III)−OH species [the OH-rebound pathway (Scheme 1A)].[2] The chemistry of several less well-studied Fe/2OG enzymes, however, does not appear to utilize the "canonical" OH-rebound mechanism. Examples of such transformations include halogenation[3−5] (e.g., CytC3, SyrB2, and WelO5), desaturation involving cleavage of two C−H bonds[6,7] (e.g., AsqJ and CarC), and C−O bond formation leading to epoxide and endoperoxide[6,8,9] (e.g., AsqJ, H6H, and Ftmox1). The oxidative decarboxylations, recently found in vinyl isonitrile and ethylene production pathways, represent new types of Fe/2OG enzyme activity. Compared to ethylene production,[10] the underlying reaction mechanism of vinyl isonitrile biosynthesis is poorly understood.[11,12]

We have recently shown that the isonitrile-containing L-tryptophan precursor (**1**) is a substrate for both the *trans*-indolyl vinyl isonitrile (**3**) synthase IsnB and the *cis*-indolyl vinyl isonitrile (**4**) synthase AmbI3.[11−13] The stereoselective formation of **3** and **4** catalyzed by IsnB and AmbI3 is accompanied by the net loss of a hydride at the benzylic carbon of **1** and the elimination of CO_2[11−13] (Scheme 1B). The IsnB/AmbI3-mediated olefination is distinct from the reactions catalyzed by other Fe/2OG desaturases in which C=C bond formation involves two consecutive C−H bond cleavages.[2] Toward this end, several mechanistic proposals can be formulated for IsnB/AmbI3-type desaturases. We and others

Scheme 1. (A) Representation of Hydroxylation Catalyzed by Fe/2OG Enzymes, (B) Decarboxylation-Assisted Desaturation Catalyzed by IsnB, AmbI3, and Other Fe/2OG Enzymes (left) and Outcomes of IsnB- and AmbI3-Catalyzed Stereoselective Vinyl Isonitrile Production (right), (C) Possible Pathways for Decarboxylation-Assisted Olefination, and (D) Substrates and Analogues Used in This Study

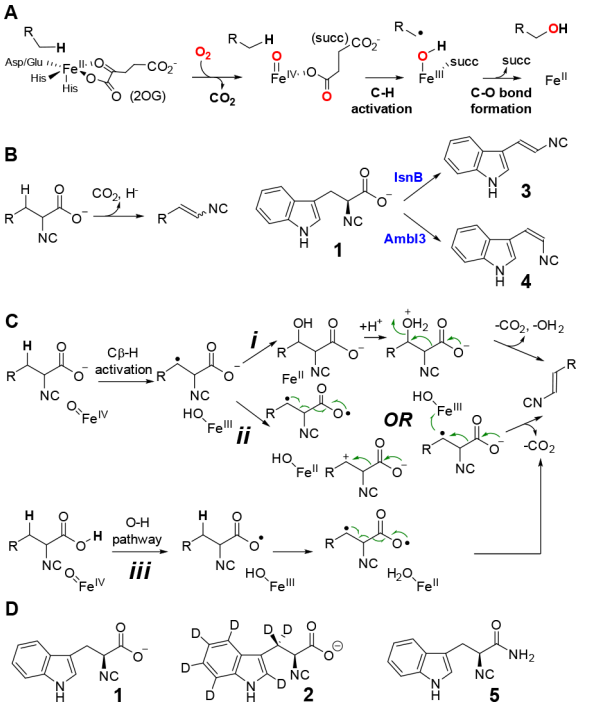

Received: January 31, 2018
Revised: February 27, 2018
Published: February 27, 2018

DOI: 10.1021/acs.biochem.8b00115
Biochemistry XXXX, XXX, XXX−XXX

have previously proposed a pathway involving HAT by a putative Fe(IV)−oxo species followed by subsequent OH rebound to produce a hydroxylated intermediate, with dehydration assisted by decarboxylation to produce the olefin and CO_2[13,14] (Scheme 1C, pathway *i*). On the other hand, inspired by recent mechanistic studies of Fe/2OG enzymes,[1,2] other mechanistic possibilities can be envisioned such as those involving a substrate radical or a cation intermediate. Similar pathways have been suggested for the cytochrome P-450 enzyme, OleT,[15] the non-heme iron enzyme, UndA,[16] and the radical SAM-dependent enzyme, MftC[17] (Scheme 1C, pathway *ii*). A third possibility, although less likely, may involve a pathway that utilizes O−H bond activation followed by a C−C bond scission and a C−H bond cleavage (Scheme 1C, pathway *iii*). To elucidate the catalytic mechanisms of IsnB and AmbI3, we prepared substrate **1**, its deuterated analogue (**2**), product standards **3** and **4**, and amide analogue **5**. IsnB and AmbI3 reactions were characterized using transient state kinetics, Mössbauer spectroscopy, and liquid chromatography with mass spectrometry (LC−MS).

Transient state kinetics via stopped-flow optical absorption spectroscopy (SF-Abs) were employed to reveal intermediates during IsnB and AmbI3 catalysis. Reactions were initiated by rapid mixing of the anaerobic IsnB (or AmbI3)·Fe(II)·2OG·**1** (or **2**) complex with an equal volume of oxygenated buffer at 5 °C with final concentrations of ∼0.5 mM O_2, 0.3 mM enzyme, 0.27 mM Fe(II), 2.7 mM 2OG, and 0.68 mM substrate. The IsnB·Fe(II)·2OG·**1** complex exhibits a broad absorption band centered at ∼540 nm that can be assigned to the Fe(II)−2OG metal-to-ligand charge transfer (MLCT) band commonly observed with Fe(II)/2OG enzymes (Figure S6).[18] After mixing, the MLCT band was depleted over ∼1 s and two stages of MLCT band decay were observed (Figure 1a). Before

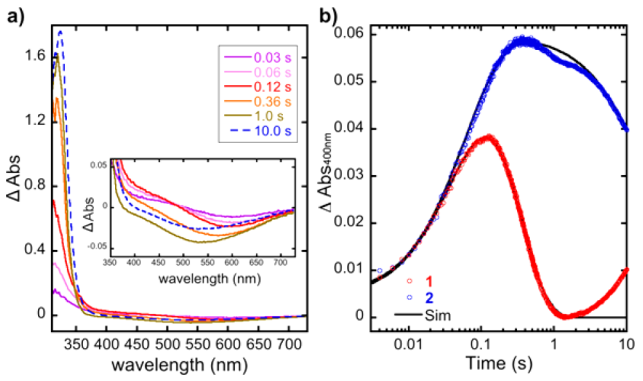

Figure 1. Kinetic evidence for C_β−H activation in IsnB catalysis. (a) Changes in absorbance at the indicated reaction times after mixing the IsnB·Fe(II)·2OG·**1** complex with O_2. The spectra at the indicated time points were obtained by subtracting the spectrum at 0.002 s. (b) Kinetic traces at 400 nm used to indicate the formation and decay of the Fe(IV)−oxo intermediate in the reactions using **1** (red) or **2** (blue), with simulations colored black. The SF-Abs results of the AmbI3 reaction are shown in Figure S9.

0.1 s, the absorption decreased near 600 nm with a concomitant increase in absorption near 320 nm. The isosbestic point observed at ∼480 nm in the difference spectra suggests a conversion of the IsnB·Fe(II)·2OG·**1** complex to a reactive intermediate. We tentatively assign this intermediate as an Fe(IV)−oxo species based on similar absorption changes observed in several well-characterized Fe/2OG enzymes.[19,20]

In the second stage of MLCT decay (>0.1 s postmixing), the magnitudes of the features in the 400−700 nm region decrease, suggesting the disappearance of the IsnB·Fe(II)·2OG·**1** and Fe(IV)−oxo complexes. Simultaneously, the absorbance at 320 nm continues to increase, which can be attributed to the formation of product **3** (Figure S16). The negative absorption feature of the MLCT band after 1 s implies that the IsnB·Fe(II)·2OG·**1** complex was largely depleted. The partial re-formation of the Fe(II)−2OG MLCT band is further observed up to 10 s, which could be attributed to the re-formation of the IsnB·Fe(II)·2OG complex due to the depletion of O_2 and/or substrate.

The time-dependent changes of the absorption at 400 nm (Figure 1b) were analyzed using a two-step kinetic model [enzyme−substrate complex + O_2 → Fe(IV)−oxo → enzyme−product complex (see the Supporting Information for more discussion)] that has been used in other Fe/2OG enzymes.[19] The 320 nm trace normally selected to analyze Fe(IV)−oxo kinetics[19,21] is not used here because of the interference of product absorption at ∼320 nm (Figure S16). The rate constants for the formation and decay of the Fe(IV)−oxo intermediate were simulated to be ∼30 mM^{-1} s^{-1} and 4.0 ± 0.2 s^{-1}, respectively, and are similar to those of reported Fe/2OG enzymes, such as TauD, SyrB2, and CarC.[4,19,21] When **2** was used, the rate of Fe(IV)−oxo formation was not perturbed (Figure 1 and Figures S7 and S8); however, the lifetime of the Fe(IV)−oxo intermediate was greatly extended (Figure 1b, blue trace), and the intermediate did not fully decay up to ∼30 s (Figure S8). Thus, the observed rate constant for Fe(IV)−oxo decay is reduced to 0.05 ± 0.01 s^{-1}. When AmbI3 was examined, analogous results were obtained where the rate constants for Fe(IV)−oxo formation and decay were found to be ∼55 mM^{-1} s^{-1} and 13 ± 1 s^{-1}, respectively, when **1** was used or ∼55 mM^{-1} s^{-1} and 0.25 ± 0.05 s^{-1}, respectively, when **2** was used (Figure S9). The greater accumulation and slow decay of the Fe(IV)−oxo species when **2** was used are likely due to the H/D kinetic isotope effect (H/D KIE of ∼80 for IsnB and ∼50 for AmbI3) on the C−H activation step, which has been documented in several Fe/2OG enzymes.[2,20,21] Together, these results support the hypothesis that an Fe(IV)−oxo species is responsible for initiating the benzylic C−H activation in IsnB and AmbI3.

To corroborate the results obtained from the SF-Abs studies, freeze-quench coupled Mössbauer experiments were performed (see the Supporting Information for more discussion). The IsnB·Fe(II)·2OG·**1** (or **2**) complex exhibited a quadrupole doublet in the Mössbauer spectrum measured at 4.2 K with an isomer shift (δ) of 1.24 mm/s and a quadrupole splitting ($|\Delta E_Q|$) of 3.09 mm/s, which is typical for high-spin ferrous species (Figure 2). In addition to this species that represents ∼75% of the total iron in the sample, the remaining 25% of the iron in the sample belonged to a species exhibiting a quadrupole doublet with a δ of 0.24 mm/s and a $|\Delta E_Q|$ of 0.54 mm/s. The high-field measurement revealed that this species has a diamagnetic ground state ($S = 0$) with parameters resembling those of isonitrile−iron(II) complexes (Figure S13 and Table S3). Therefore, we reasoned that this minor species originates from the coordination of the isonitrile group of **1** to the Fe(II) center. Following addition of O_2, it remains unchanged (Table S2). Thus, it is not involved in IsnB catalysis. The Mössbauer spectra of samples quenched at various time points after mixing with oxygenated buffer revealed the accumulation of an Fe(IV)−oxo intermediate,

DOI: 10.1021/acs.biochem.8b00115
Biochemistry XXXX, XXX, XXX−XXX

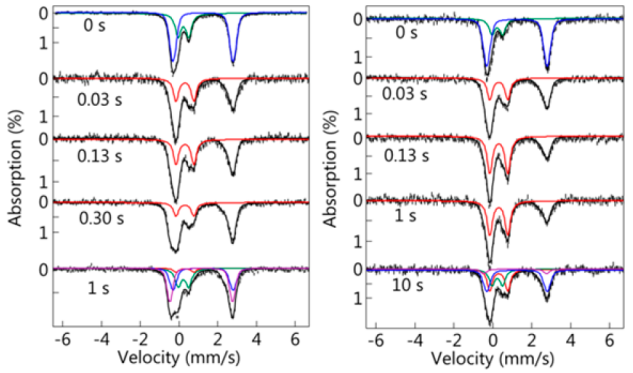

Figure 2. 4.2 K zero-field Mössbauer spectra of the IsnB reaction. The black hashed lines represent spectra of samples freeze quenched at various time points by rapid mixing of the IsnB·Fe(II)·2OG·substrate complex (**1**, left; **2**, right) with O_2. The red, green, blue, and purple lines represent the spectral simulations of the Fe(IV)−oxo species, the isonitrile−Fe(II) complex, the enzyme−substrate complex, and the enzyme−product complex. The black lines represent the overall simulations.

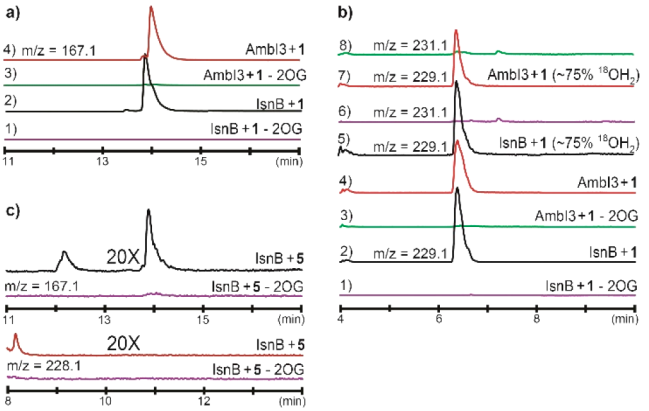

Figure 3. LC−MS analysis of IsnB and AmbI3 catalysis. (a) Formation of **3** and **4** when reacting **1** with IsnB and AmbI3. (b) **1**−OH formation when **1** was reacted with IsnB or AmbI3 (m/z 213.1 → 229.1, traces 1−4). In the presence of ~75% $H_2{}^{18}O$, no ^{18}O incorporation was detected (m/z 231.1, traces 5−8). (c) Formation of **3** and the **5**−OH product (m/z 212.1 → 228.1) (top and bottom, respectively) when **5** was reacted with IsnB. Because of the poor reactivity of **5**, traces are enlarged by 20 times (20×).

which is evidenced by the observation of a quadrupole doublet with a δ of 0.31 mm/s and a $|\Delta E_Q|$ of 0.92 mm/s. The Fe(IV)−oxo species accumulated to a maximum of ~28% of the total iron in the sample quenched at 0.13 s and decayed to <4% at 1 s. In addition, a quadrupole doublet representing another high-spin ferrous species with a δ of 1.15 mm/s and a $|\Delta E_Q|$ of 3.24 mm/s was formed in a process that was concomitant with the decay of the Fe(IV)−oxo species. This quadrupole doublet is different from the substrate-bound complex and likely represents the IsnB·Fe(II)·product complex. When **2** was used, the amount of Fe(IV)−oxo species observed at 0.03 s was similar (~25%) to that in the case of **1**; however, it accumulated to a higher level (~45%) at 0.13 s and hardly decayed at 1 s. In a sample quenched at 10 s, the Fe(IV)−oxo species still accounted for ~20% of the total iron. These observations are consistent with the results of the SF-Abs experiments in that a large H/D KIE is observed for the decay of the Fe(IV)−oxo species (Figure S10).

Product distributions for IsnB and AmbI3 reactions with **1**, **2**, and **5** were characterized using LC−MS. Analogous to the condition for the SF-Abs experiment, the IsnB (or AmbI3)·Fe(II)·2OG complex was incubated with the substrate anaerobically and then mixed with an equal volume of oxygenated buffer with final concentrations of 0.12 mM enzyme, 0.1 mM Fe(II), 0.5 mM substrate, 1.0 mM 2OG, and ~0.5 mM O_2. After 5 min, the reaction mixtures were subjected to LC−MS. In addition to the desaturated products (**3** for IsnB and **4** for AmbI3), a minor peak corresponding to a hydroxylated **1** (**1**−OH) in both reactions was detected [mass shift of +16, m/z 229.1 (Figure 3a,b)]. The ratio of **1**−OH to **3** or **4** is ~1.0:5.6. We reasoned that **1**−OH could originate from either a hydroxylated intermediate prior to decarboxylation (e.g., as in Scheme 1C, pathway ***i***) or an off-pathway product generated by quenching of a reactive intermediate, such as a benzylic cation or radical (Scheme 1C, pathway ***ii***). To distinguish these possibilities, we performed the reactions in buffer enriched with $H_2{}^{18}O$ (~75% $H_2{}^{18}O$). In both reactions, the $^{16}O/^{18}O$ product ratio is >99:1 (Figure 3b). Thus, the oxygen atom of **1**−OH is likely derived from O_2, which is consistent with the OH-rebound pathway. Although this observation disfavors the pathway in which quenching of reactive species yields **1**−OH, it cannot distinguish whether **1**−OH is the intermediate used for decarboxylation or a product resulting from residual hydroxylase activity.

To probe whether the hydroxylated species is an on-pathway or an off-pathway product, an amide analogue **5** was prepared. By replacing the carboxylate with an amide that cannot easily undergo hydroxylation-induced decarboxylation, we anticipate that the rate of IsnB- and AmbI3-catalyzed production of **3** and **4**, respectively, would decrease with **5** and the hydroxylated intermediate would accumulate if the hydroxylation/decarboxylation pathway is being used. In contrast, if desaturation does not proceed through this pathway, we would not observe an increased level of the hydroxylated product. When **5** was incubated with IsnB, **3** was still produced. Additionally, a peak with the m/z value corresponding to that of hydroxylated **5** (**5**−OH) was detected (m/z 228.1), and the ratio of **5**−OH to **3** is ~1:6 (Figure 3c). In the absence of 2OG, neither **3** nor **5**−OH was formed. When AmbI3 was tested, no obvious substrate consumption or product formation could be detected. Although IsnB can catalyze the production of **3** and **5**−OH, the reactivity is only ~5% compared to that of **1**. We speculate that the binding affinity of **5** for IsnB and AmbI3 is very poor. While the LC−MS results suggest that the hydroxylated product likely originates from an OH-rebound pathway, the lack of enhancement of the hydroxylated product when **5** was used indicates that it is likely an off-pathway product during IsnB reaction.

In conclusion, our results suggest that the catalytic strategy of utilizing an Fe(IV)−oxo intermediate to trigger benzylic C−H bond activation is operative in IsnB and AmbI3 catalysis. The following steps diverge from the canonical OH-rebound pathway in which desaturation is likely to proceed through a pathway involving a benzylic radical or a benzylic carbocation intermediate. An analogous pathway utilizing single-electron transfer to the Fe(III)−OH species to produce a substrate cation or a diradical intermediate has been proposed in the H_2O_2-dependent cytochrome P-450 enzyme, OleT, and O_2-dependent non-heme iron enzyme, UndA,[15,16,22] which implies a common reaction mechanism for decarboxylation-assisted olefination may exist among different types of O_2/H_2O_2 activating enzymes.

DOI: 10.1021/acs.biochem.8b00115
Biochemistry XXXX, XXX, XXX−XXX

■ ASSOCIATED CONTENT

Supporting Information

The Supporting Information is available free of charge on the ACS Publications website at DOI: 10.1021/acs.biochem.8b00115.

Methods, Figures S1−S16, Tables S1−S3, and references (PDF)

■ AUTHOR INFORMATION

Corresponding Authors

*E-mail: wchang6@ncsu.edu.

*E-mail: ysguo@andrew.cmu.edu.

*E-mail: xinyuliu@pitt.edu.

ORCID

Yisong Guo: 0000-0002-4132-3565

Wei-chen Chang: 0000-0002-2341-9846

Author Contributions

J.-L.H. and Y.T. contributed equally to this work.

Funding

This work was supported by grants from North Carolina State University, grants from Carnegie Mellon University, and National Science Foundation Grant CHE-1654060 (to Y.G.).

Notes

The authors declare no competing financial interest.

■ REFERENCES

(1) Tang, M. C., Zou, Y., Watanabe, K., Walsh, C. T., and Tang, Y. (2017) Oxidative Cyclization in Natural Product Biosynthesis. *Chem. Rev. 117*, 5226−5333.

(2) Martinez, S., and Hausinger, R. P. (2015) Catalytic Mechanisms of Fe(II)- and 2-Oxoglutarate-dependent Oxygenases. *J. Biol. Chem. 290*, 20702−20711.

(3) Galonic, D. P., Barr, E. W., Walsh, C. T., Bollinger, J. M., Jr., and Krebs, C. (2007) Two interconverting Fe(IV) intermediates in aliphatic chlorination by the halogenase CytC3. *Nat. Chem. Biol. 3*, 113−116.

(4) Matthews, M. L., Krest, C. M., Barr, E. W., Vaillancourt, F. H., Walsh, C. T., Green, M. T., Krebs, C., and Bollinger, J. M. (2009) Substrate-triggered formation and remarkable stability of the C-H bond-cleaving chloroferryl intermediate in the aliphatic halogenase, SyrB2. *Biochemistry 48*, 4331−4343.

(5) Mitchell, A. J., Zhu, Q., Maggiolo, A. O., Ananth, N. R., Hillwig, M. L., Liu, X., and Boal, A. K. (2016) Structural basis for halogenation by iron- and 2-oxo-glutarate-dependent enzyme WelO5. *Nat. Chem. Biol. 12*, 636−640.

(6) Ishikawa, N., Tanaka, H., Koyama, F., Noguchi, H., Wang, C. C., Hotta, K., and Watanabe, K. (2014) Non-heme dioxygenase catalyzes atypical oxidations of 6,7-bicyclic systems to form the 6,6-quinolone core of viridicatin-type fungal alkaloids. *Angew. Chem., Int. Ed. 53*, 12880−12884.

(7) McGowan, S. J., Sebaihia, M., Porter, L. E., Stewart, G. S., Williams, P., Bycroft, B. W., and Salmond, G. P. (1996) Analysis of bacterial carbapenem antibiotic production genes reveals a novel beta-lactam biosynthesis pathway. *Mol. Microbiol. 22*, 415−426.

(8) Hashimoto, T., Matsuda, J., and Yamada, Y. (1993) Two-step epoxidation of hyoscyamine to scopolamine is catalyzed by bifunctional hyoscyamine 6 beta-hydroxylase. *FEBS Lett. 329*, 35−39.

(9) Yan, W., Song, H., Song, F., Guo, Y., Wu, C. H., Sae Her, A., Pu, Y., Wang, S., Naowarojna, N., Weitz, A., Hendrich, M. P., Costello, C. E., Zhang, L., Liu, P., and Zhang, Y. J. (2015) Endoperoxide formation by an alpha-ketoglutarate-dependent mononuclear non-haem iron enzyme. *Nature 527*, 539−543.

(10) Martinez, S., and Hausinger, R. P. (2016) Biochemical and Spectroscopic Characterization of the Non-Heme Fe(II)- and 2-Oxoglutarate-Dependent Ethylene-Forming Enzyme from Pseudomonas syringae pv. phaseolicola PK2. *Biochemistry 55*, 5989−5999.

(11) Brady, S. F., and Clardy, J. (2005) Cloning and heterologous expression of isocyanide biosynthetic genes from environmental DNA. *Angew. Chem., Int. Ed. 44*, 7063−7065.

(12) Brady, S. F., and Clardy, J. (2005) Systematic investigation of the Escherichia coli metabolome for the biosynthetic origin of an isocyanide carbon atom. *Angew. Chem., Int. Ed. 44*, 7045−7048.

(13) Chang, W.-c., Sanyal, D., Huang, J. L., Ittiamornkul, K., Zhu, Q., and Liu, X. (2017) In Vitro Stepwise Reconstitution of Amino Acid Derived Vinyl Isocyanide Biosynthesis: Detection of an Elusive Intermediate. *Org. Lett. 19*, 1208−1211.

(14) Zhu, J., Lippa, G. M., Gulick, A. M., and Tipton, P. A. (2015) Examining Reaction Specificity in PvcB, a Source of Diversity in Isonitrile-Containing Natural Products. *Biochemistry 54*, 2659−2669.

(15) Grant, J. L., Hsieh, C. H., and Makris, T. M. (2015) Decarboxylation of fatty acids to terminal alkenes by cytochrome P450 compound I. *J. Am. Chem. Soc. 137*, 4940−4943.

(16) Rui, Z., Li, X., Zhu, X., Liu, J., Domigan, B., Barr, I., Cate, J. H., and Zhang, W. (2014) Microbial biosynthesis of medium-chain 1-alkenes by a nonheme iron oxidase. *Proc. Natl. Acad. Sci. U. S. A. 111*, 18237−18242.

(17) Bruender, N. A., and Bandarian, V. (2016) The Radical S-Adenosyl-l-methionine Enzyme MftC Catalyzes an Oxidative Decarboxylation of the C-Terminus of the MftA Peptide. *Biochemistry 55*, 2813−2816.

(18) Pavel, E. G., Zhou, j., Busby, R. W., Gunsior, M., Townsend, C. A., and Solomon, E. I. (1998) Circular Dichroism and Magnetic Circular Dichroism Spectroscopic Studies of the Non-Heme Ferrous Active Site in Clavaminate Synthase and Its Interaction with α-Ketoglutarate Cosubstrate. *J. Am. Chem. Soc. 120*, 743−753.

(19) Price, J. C., Barr, E. W., Tirupati, B., Bollinger, J. M., Jr., and Krebs, C. (2003) The first direct characterization of a high-valent iron intermediate in the reaction of an alpha-ketoglutarate-dependent dioxygenase: a high-spin FeIV complex in taurine/alpha-ketoglutarate dioxygenase (TauD) from Escherichia coli. *Biochemistry 42*, 7497−7508.

(20) Price, J. C., Barr, E. W., Glass, T. E., Krebs, C., and Bollinger, J. M., Jr. (2003) Evidence for hydrogen abstraction from C1 of taurine by the high-spin Fe(IV) intermediate detected during oxygen activation by taurine:alpha-ketoglutarate dioxygenase (TauD). *J. Am. Chem. Soc. 125*, 13008−13009.

(21) Chang, W.-c., Guo, Y., Wang, C., Butch, S. E., Rosenzweig, A. C., Boal, A. K., Krebs, C., and Bollinger, J. M., Jr. (2014) Mechanism of the C5 stereoinversion reaction in the biosynthesis of carbapenem antibiotics. *Science 343*, 1140−1144.

(22) Grant, J. L., Mitchell, M. E., and Makris, T. M. (2016) Catalytic strategy for carbon-carbon bond scission by the cytochrome P450 OleT. *Proc. Natl. Acad. Sci. U. S. A. 113*, 10049−10054.

DOI: 10.1021/acs.biochem.8b00115
Biochemistry XXXX, XXX, XXX−XXX